JOURNAL OF THE AMERICAN CHEMICAL SOCIETY

Article

pubs.acs.org/JACS

Three-Dimensional DNA Crystals with pH-Responsive Noncanonical Junctions

Stephanie E. Muser and Paul J. Paukstelis*

Department of Chemistry and Biochemistry, Center for Biomolecular Structure and Organization, University of Maryland, Maryland NanoCenter, College Park, Maryland 20742, United States

Supporting Information

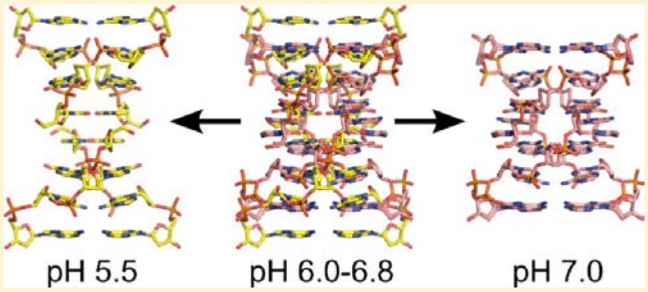

ABSTRACT: Three-dimensional (3D) DNA crystals have been envisioned as programmable biomaterial scaffolds for creating ordered arrays of biological and nonbiological molecules. Despite having excellent programmable properties, the linearity of the Watson−Crick B-form duplex imposes limitations on 3D crystal design. Predictable noncanonical base pairing motifs have the potential to serve as junctions to connect linear DNA segments into complex 3D lattices. Here, we designed crystals based on a template structure with parallel-stranded noncanonical base pairs. Depending on pH, the structures we determined contained all but one or two of the designed secondary structure interactions. Surprisingly, a conformational change of the designed Watson−Crick duplex region resulted in crystal packing differences between the predicted and observed structures. However, the designed noncanonical motif was virtually identical to the template when crystals were grown at pH 5.5, highlighting the motif's predictability. At pH 7.0 we observed a structurally similar variation on this motif that contains a previously unobserved C−G•G−C quadruple base pair. We demonstrate that these two variants can interconvert *in crystallo* in response to pH perturbations. This study spotlights several important considerations in DNA crystal design, describes the first 3D DNA lattice composed of A-DNA helical sheets, and reveals a noncanonical DNA motif that has adaptive features that may be useful for designing dynamic crystals or biomaterial assemblies.

■ INTRODUCTION

The ability for complementary oligonucleotide sequences to recognize each other in complex sequence environments has made DNA an ideal molecule for programmed self-assembly. This property has been used to generate discrete nanoscale DNA objects in two and three dimensions,[1−9] to perform computations,[10−13] and to organize nonbiological materials.[14−18] Creating periodic 3D DNA arrays, or crystals, has been recognized as a major goal toward applying DNA lattices as macromolecular scaffolds for nanotechnology applications.[19] On the microscale, biomolecules and biomimetics, including DNA, have been used to create biomaterials for use in separations, controlled drug delivery and release, diagnostics, and as interfacial materials between biological and inorganic realms.[20−24] A major focus of these efforts has been to develop adaptive materials that are capable of undergoing predictable, conformational changes in response to local environmental changes as a way to enhance their utility and functionality.

While DNA has many favorable self-assembly characteristics, it has one major drawback for 3D self-assembly: the Watson−Crick DNA helix is topologically linear. The ability to form complex periodic 3D structures from DNA requires branching from these lines.[25] Branched DNAs occur naturally during recombination in the form of Holliday junctions, and several designs have used asymmetric sequences to create nonmigratory branched junctions.[26] These multiple-crossover motifs have been designed to self-assemble in a variety of periodic 2D arrays based on the Watson−Crick pairing of sticky ends (reviewed in ref 8). More recently, sophisticated nonperiodic 3D objects have been constructed using DNA origami techniques.[27−34] Collectively, these constructs have successfully illustrated the power of DNA self-assembly to create nanostructures, but to date only one crystal design of a completely Watson−Crick 3D DNA array has been described at low resolution.[9]

Predictable non-Watson−Crick motifs have the potential to create branched structures that could be incorporated into the rational design of 3D DNA structures.[35] Isolated non-Watson−Crick base pairs can readily form in the absence of opportunities for Watson−Crick pairing or in favorable environments. Non-Watson−Crick pairings can also provide structural diversity that in some cases is required for biological function. Nonstandard base pairs play crucial roles in the functional tertiary structures for RNA molecules.[36] For DNA, G-quadruplex motifs are found in the telomeric repeats of chromosomes[37] and have also been shown to be involved in transcriptional regulation within gene promoters.[38] Though

Received: March 14, 2012
Published: July 7, 2012

there are only a limited number of known non-Watson−Crick motifs, these are beginning to find uses in DNA nanotechnology, primarily for nanomechanical devices and sensors.[39−42]

Several crystal structures have demonstrated the potential for noncanonical base pairs in 3D DNA crystal design. The first example of a continuously base paired 3D lattice was reported from the crystal structure of the 13-mer, d-(GGACAGATGGGAG),[43] in which a single molecule interacts with symmetry related strands to form columns of coaxially stacked B-form duplexes that are held together at the sites of stacking through parallel homopurine base pairs between 5′-$G_1G_2A_3$ of one strand and 5′-$G_{10}G_{11}A_{12}$ in another strand. This noncanonical motif was used to design crystals containing elongated duplex regions and resulted in crystals with large solvent channels that were capable of functioning as macromolecular sieves.[44] The observation of identical 5′-GGA base pairs in solution[45] has suggested that these homoparallel base pairs can form a predictable noncanonical motif.

DNAs containing the sequence 5′-CGA have also been observed to form parallel-stranded homobase pairs.[46−49] This 5′-CGA homoparallel motif is structurally related to the 5′-GGA motif, though it contains a symmetric hemiprotonated C•C base pair instead of an asymmetric G(*syn*)•G(*anti*) base pair at the 5′-position. Both motifs derive much of their stability from interstrand stacking of the second and third base pairs. The first crystal structure of the 5′-CGA parallel-stranded motif was described for the molecule d(GCGAAAGCT).[46] One molecule in the asymmetric unit forms intermolecular base pairs in both noncanonical and Watson−Crick regions (Figure 1A). The noncanonical motif in this structure is a variation of the 5′-CGA parallel motif characterized in solution[47,48] in that it was formed from the 5′-CGAA region of two strands with the additional A•A pair forming through symmetric N1−N6 bonding of the Watson−Crick face. Following this additional pairing, the backbone takes a sharp turn to form a short B-DNA duplex region with four self-complementary base pairs (Figure 1A). The helical axis of this duplex is coincident with the 4_1 screw axis, resulting in the 5′-CGAA parallel motif jutting out orthogonally from these columns of pseudoinfinitely stacked Watson−Crick helices (Figure 1B). These helical columns are assembled into a 3D lattice by stacking interactions between two C_2•C_2 base pairs to form noncanonical junctions between the columns.

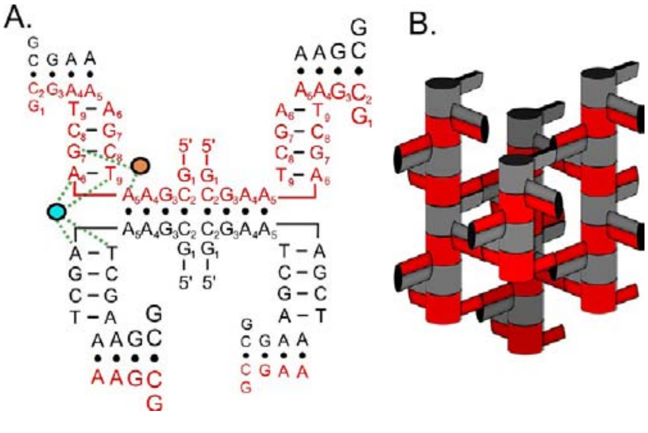

Figure 1. Nonamer template structure. (A) Secondary structure of the crystal lattice used as the template for the crystals described here.[46] Watson−Crick base pairs are represented with dashes, and noncanonical base pairs are shown with filled black spheres. Ion binding sites observed in the structure are shown as colored spheres (CoHex: orange; Mg^{2+}: blue) with nucleotide interactions shown by dashed lines. For the noncanonical regions, increasing and decreasing letter size represents bases coming 90° out or into the plane of the page, respectively. (B) Cylindrical representation of the template lattice. Red and black cylinders represent duplex regions that stack vertically end-to-end on the 4_1 screw axis. The noncanonical 5′-CGAA junctions extend out orthogonally from these cylinders. Stacking between the noncanonical regions generates a 3D DNA lattice with an internal network of solvent channels.

Here, we describe crystal structures of d-(GCGAAAGGGCACGTGCCCT) based on the interactions seen in the d(GCGAAAGCT) nonamer structure. Our approach was to make an expansion of the self-complementary B-form duplex region to generate crystals with altered unit cell dimensions along the four-fold symmetry axis. Crystals grown at different pH's resulted in structures that contained all but one or two of the designed secondary structure interactions. However, these crystals had a different overall lattice organization than we had anticipated. Most dramatically, the Watson−Crick duplex region adopted an A-form conformation, resulting in the formation of woven helical sheets as opposed to the expected stacked helical columns. Despite unanticipated differences in the duplex region, at pH 5.5 all of the predicted noncanonical base pairs were observed and were identical to the template structure. At neutral pH the hemiprotonated C_2•C_2 pair was absent. Under these conditions the cytosines instead formed Watson−Crick base pairs with two stacked G•G pairs to generate a previously unobserved four-stranded C−G•G−C quadruple base pair at the junction. Finally, we demonstrate that these junction types can interconvert *in crystallo* in response to pH changes, suggesting that this motif type may be a novel DNA primitive for creating adaptive biomaterials.

RESULTS AND DISCUSSION

Crystal Design and Secondary Structure. We designed the crystal lattice to maintain the interactions of the 5′-CGAA homoparallel motif and to extend the Watson−Crick duplex region by approximately one helical turn through the addition of 10 self-complementary nucleotides. Figure 2A shows the predicted secondary structure of this expanded lattice. Several structural features of the nonamer template influenced our sequence design. First, we kept the nucleotide identities of the first and last base pairs of the duplex region identical to the template sequence and inserted the additional nucleotides between the central G−C pairs. Ion binding sites in both the major and minor grooves of the short duplex region suggested that base-specific recognition at the duplex ends stabilized the backbone transition between regions (Figure 1A). Most significant was the presence of a bound cobalt(III) hexammine ion (CoHex) in the major groove at the G_7 position of the nonamer that supports the bending at the junction between the parallel and antiparallel regions.[46] Further, water-mediated coordination of Mg^{2+} at the terminal A_6−T_9 pair was observed in the shared minor groove where these base pairs stack to form a pseudocontinuous helix. We also reasoned that the end-to-end helical stacking between Watson−Crick duplex regions resembled a discontinuous AT dinucleotide step and that the identities at this position may be necessary to facilitate crystal packing. Finally, the edge-to-face stacking of the A_6−T_9 pairs to the A_5−A_5 parallel base pairs brings the T_9 C5-methyls in proximity to the A_5 sugars where they could stabilize the tight

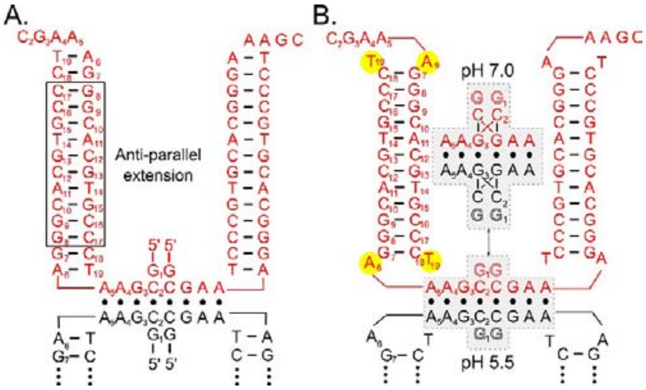

Figure 2. Predicted and observed secondary structures. (A) The predicted secondary structure of the designed expanded lattice. The self-complementary antiparallel extension was added between the base pairs present in the template nonamer. The observed secondary structures of the final structures are shown in (B). The antiparallel duplex regions are identical at the two pH's. At pH 5.5 the crystallographic two-folds intersect between the stacked $C_2 \bullet C_2$ pairs, while at pH 7.0 they intersect between the stacked C−G•G−C quadruple base pairs. At both pH's the predicted A_6−T_{19} pair in the antiparallel duplex region was not formed (yellow). G_1 was not observed at either pH.

turn between parallel and antiparallel regions. The additional nucleotides in the antiparallel extension were chosen to be self-complementary and to avoid possible Watson−Crick pairings with nucleotides from the parallel region.

Sitting drop vapor diffusion in conditions similar to those used to crystallize the nonamer oligonucleotide resulted in plate-like crystals that generally grew in clusters. Variation of the crystallization conditions showed that crystal formation was dependent on CoHex and Mg^{2+}, but independent of pH ranging from 4.5 to 7.4 using sodium cacodylate and acetate buffers. The crystals grew in space group *I*222 with common *a* and *b* cell constants. For the *c* cell constants, crystals grown at pH 5.5 or below were ~85 Å, while crystals grown at pH 7.0 or above were ~73 Å. The crystals diffracted to better than 2.0 Å at these pH's and were readily phased by single-wavelength anomalous dispersion from bound CoHex ions. Data collection and refinement statistics for crystals grown at pH 5.5 and pH 7.0 are given in Table S1. As anticipated, the structures contained one DNA 19-mer in the asymmetric units with symmetry related strands forming both an antiparallel Watson−Crick duplex and a parallel noncanonical junction. The secondary structures of the determined crystal structures are shown in Figure 2B.

Antiparallel Duplex Region. The antiparallel duplex region was designed as a self-complementary B-DNA helix with 7 unique base pairs to form a 14 base pair duplex (Figure 2A). At both pH's we observed only 6 of the 7 unique pairs, with A_6 and T_{19} forming stacking interactions with symmetry related strands rather than base pairs with each other (Figure 2B). The electron density for this region was well-defined with purines and pyrimidines readily distinguishable in experimentally phased electron density maps (Figure S1). The duplex regions in the crystals solved at the two pH's were virtually identical with an rmsd of 0.087 Å for residues 6 through 19.

Quite unexpectedly, the Watson−Crick duplex region adopted an A-form conformation rather than the B-form duplex that our crystal design was predicated upon. The helix and base pairing parameters analyzed with 3DNA[50] showed the duplex region to have typical A-form values with several slight deviations in intrastrand phosphate distances and sugar puckers. The relatively short P−P distance (5.5 Å) between G_7 and G_8 was the result of two CoHex ions in the major groove of the duplex (Figure 3). CoHex1 amines make direct hydrogen bonding contact with O6 and N7 of G_8 and O6 of G_9. Additionally, CoHex1 contacts the G_7 phosphate and makes water-mediated contacts with N7 of the G_7 base. CoHex2 does not make any base-specific contacts, but occupies a position between the G_7 and G_8 phosphates to provide charge shielding that accounts for the shortened intrastrand P−P distance. CoHex2 simultaneously contacts the C_{12} phosphate to bridge and collapse the major groove. CoHex2 also interacts with the C_{18} phosphate from a symmetry related strand to help stabilize interactions between A-DNA duplex regions in the crystal (see below). Interestingly, the two CoHex ions are themselves relatively close together, with only 3.5 Å between the closest amines.

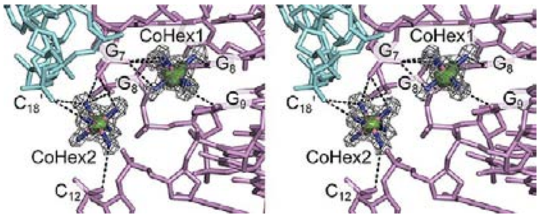

Figure 3. Ion binding in the A-DNA major groove. Stereoview of the duplex major groove at the CoHex binding site of the pH 7.0 structure. Dashed black lines represent interactions between CoHex ions and the DNA. Sigma-A-weighted $2F_o-F_c$ electron density is contoured around the CoHex ions at 3σ. Anomalous difference density contoured at 7σ is rendered as a semitransparent green surface. CoHex1 makes base specific contacts with G_8 and G_9 nucleobases and with the G_7 phosphate oxygen. CoHex2 makes electrostatic interactions across the duplex major groove through phosphate contacts with G_7, G_8, and C_{12}. Additional electrostatic contacts are made with the C_{18}' phosphate from a symmetry-related duplex strand (light blue).

Dehydration is a known inducer of A-DNA,[51] and DNA crystal structures solved using high precipitant concentrations are often A-form. The crystals we describe here could be obtained over a wide range of precipitant concentrations suggesting that dehydration is not the main source of this conformational change. Previous work showed that polyamines such as spermidine, spermine, and CoHex can induce A-DNA conformational transitions, particularly for sequences that contain runs of guanosines.[52−54] The two CoHex ions that interact near a run of three guanine bases within the major groove suggests that this is a likely cause of the conformational change. The CoHex positions agree with previously suggested binding modes, sequence-specific hydrogen bonding and major groove phosphate charge shielding, that are responsible for the induced A-DNA transition.[54] CoHex1 does not appear to make significant charge shielding contributions, but the close packing of the two bound CoHex ions suggests that they may function similarly to imidizole linked cobalt(III) pentamine molecules that are effective at inducing B- to A-form conformational changes.[55]

Parallel-Stranded Noncanonical Regions. The parallel noncanonical region was designed to form the same 5′-CGAA homobase pairs observed in the nonamer template. The electron density was less well-defined for this region than for the Watson−Crick region at both pH's, but was interpretable from C_2 through A_5 (Figure S2). In all the crystals we examined, those grown at pH 7.0 or greater showed better overall density in this region than crystals grown at lower pH's. Density for the G_1 residue was not observed.

At pH 5.5, symmetry-related interactions between two strands formed the anticipated $C_2•C_2$, $G_3•G_3$, $A_4•A_4$, and $A_5•A_5$ homoparallel base pairs (Figure 2B). Superpositions of the corresponding base pairs from the nonamer structure showed that the structures were highly similar with an rmsd of 0.35 Å for all atoms from C_2 through A_5 of both strands (Figure 4A). However, the hemiprotonated $C_2•C_2$ pair was not observed in crystals examined at pH 7.0. Accordingly, the two C_2 nucleotides varied substantially in comparison to the template (rmsd: 3.23 Å), while nucleotides G_3 through A_5 of the two strands were similar (rmsd: 0.76 Å; Figure 4A).

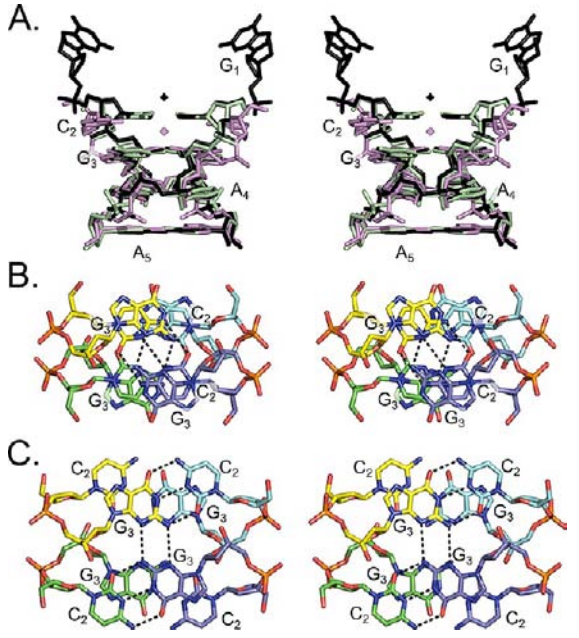

Figure 4. Noncanonical junction regions. (A) Stereoview superposition of the noncanonical base pairing regions of the nonamer template (black), pH 5.5 structure (green) and pH 7.0 structure (violet). Rmsd values for all visible atoms (excluding G_1 which was not visible in either structure solved here) were 0.35 and 1.66 Å between the template structure and pH 5.5. and pH 7.0 structures, respectively. Intersection of the crystallographic two-fold axes are shown by crossed ovals. The black ovals are shared by the nonamer template and the pH 5.5 structure, and the violet ovals are from the pH 7.0 structure. (B) Stereoview of the C•C stacked junction region at pH 5.5 with carbon atoms colored different for each of the four strands that make up the junction. Hydrogen bonds in the top unique base pairs are represented by dashed black lines. (C) Stereoview of the stacked C−G•G−C quadruple base pairs in the pH 7.0 structure. Base pairs of a single quadruple are shown as dashed black lines.

As in the nonamer template, the noncanonical regions at both pH's serve as junctions to link duplex regions. The junctions are formed by two sets of noncanonical base pairs (four DNA strands) that stack upon each other. For the structure solved at pH 5.5, the junctions stacked as predicted with crystallographic two-fold axes intersecting between stacked $C_2•C_2$ base pairs from each half of the junction (Figure 4B). For the structure solved at pH 7.0, the crystallographic two-folds intersect between the $G_3•G_3$ pairs, accounting for the shortened *c* cell constant. The stacking of two $G_3•G_3$ pairs positions C_2 from each strand to form an antiparallel Watson−Crick base pair with a G_3 nucleotide across the crystallographic two-folds. This forms two interlocked C−G•G−C quadruple base pairs that stack upon each other (Figure 4C). This mixed parallel/antiparallel quadruple base pair results in hydrogen bonding interactions between all four strands of the junction region.

Though we readily obtained crystals from pH 4.5 to 7.4, we were unable to determine structures in the intermediate pH range of 6.0 to 6.8. These crystals generally had a diffraction limit of ~3.5 Å, but they consistently showed extreme mosaicity and spot splitting consistent with multicrystal diffraction (Figure S3). A possible explanation for this behavior was the crystals having a mixed population of C•C and C−G•G−C stacked junctions at these intermediate pH's, resulting in localized changes to the *c* cell constant throughout the crystal. To examine this possibility, we transferred crystals grown at pH 6.6 to pre-equilibrated crystallization solutions at pH 4.5 or 7.4. Remarkably, after soaking at the extreme pH's for as little as 10 min the crystals diffracted to high resolution (2.0 Å) under cryocooling conditions and were readily indexed with the cell constants consistent with the formation of C•C (pH 4.5) or C−G•G−C (pH 7.4) junctions.

To further explore the influence of pH on individual crystals and gauge how rapidly the cell transition could take place, we performed room temperature data collection with pH changes induced through vapor exchange within the microcapillary environment. Crystals diffracted to lower resolution at room temperature, but they could be readily indexed with cell constants within 1−2 Å of crystals grown at the same pH and observed under cryocooling. For crystals grown at pH 7.0 with the motif conversion induced by acetic acid, oscillation images showed the appearance of new reflections within 90 s after capillary exchange, but with *c* cell constants similar or identical to those before the exchange (Figure 5). The same oscillation sweep recorded over 90−150 s after the exchange showed the appearance of split spots indicative of multicrystal diffraction, and subsequent images showed the apparent positional migration of these reflections consistent with the lengthening of the *c* cell constant through the entire crystal (Figure 5). Corresponding cell changes were obtained for crystals grown at pH 5.5 with cell shrinkage induced with ammonium hydroxide, but in this case the motif transitions were complete at the earliest time point following capillary exchange (data not shown). The apparent differential kinetics of these cell changes may be due to the strength and volatility of the pH inducers, but could also reflect intrinsic kinetic or thermodynamic properties of the junction transition. Significantly, these results demonstrate that (i) these noncanonical junctions are capable of interconversion within a single crystal in response to pH perturbations, (ii) the conversion can occur on relatively short time scales, and (iii) these changes are concerted and precise enough to maintain lattice packing and diffraction.

Other Crystal Contacts. Though almost all of the designed base pairing interactions were observed in the crystal structures, the end-to-end duplex stacking interactions were not observed. In the nonamer template, base pair stacking of the two A_6-T_9 pairs generates columns of pseudoinfinite helices (Figure 1). The equivalent base pair in the expanded lattice (A_6-T_{19}) was not formed, and consequently there is no direct stacking between the two A-form duplexes that are associated through the noncanonical base pairing. Though these two duplex regions are still coaxial with respect to helix direction, the first

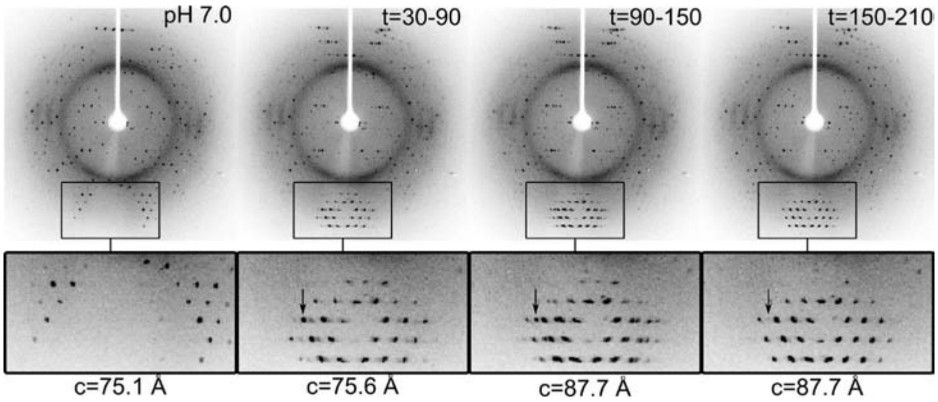

Figure 5. pH-induced structural transition in a single crystal over time. 1 min, 6° oscillation images of a pH 7.0 crystal at room temperature. Magnified boxed regions and indexed *c* cell constants using 5 I/σ reflections are shown below each full diffraction image. The image on the far left shows diffraction prior to pH perturbation. Subsequent images are of the same crystal in the same orientation following capillary exchange containing a reservoir solution with 0.1 M acetic acid. The time period in seconds following the exchange over which the image was collected is indicated. The readout time for the CCD detector (~1 s) has been ignored. Arrowheads denote the starting position of an example reflection (−2,12,−8) that appears within 90 s following exchange. This reflection resolves to the right in subsequent frames as the *c* cell constant expands throughout the crystal. Similar changes occur throughout the diffraction images demonstrating concerted crystal changes in response to pH perturbations.

base pairs of the two helices (G_7—C_{18}) are separated by 24 Å (Figure 6A). This separation allows a symmetry-related A-form duplex to reside between them. This central duplex is oriented and stabilized to the other two by interactions between the C_{18} phosphate and CoHex2 in the major groove of the flanking helices (described above), and from stacking interactions between T_{19}'s of the central duplex and the unpaired A_6's of the flanking duplexes (Figure 6B). Together, these interactions clamp the central duplex region between the two flanking helices. The nonstandard A-DNA sugar puckers (C2′-endo) of C_{17} and C_{18} appear to be induced by the proximity of A_6 and G_7 from the flanking strands.

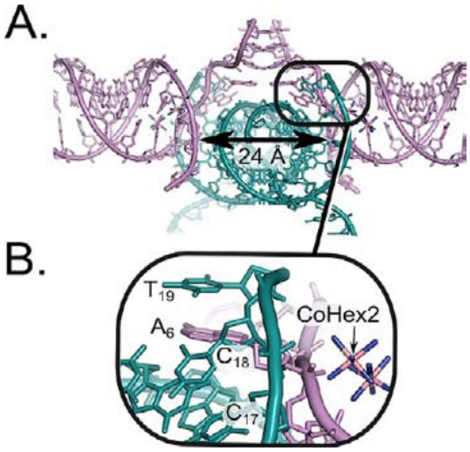

Figure 6. A-DNA helices are woven together and stabilized by stacking and electrostatic interactions. (A) Watson−Crick duplex regions that are joined through the parallel noncanonical region (violet) do not directly stack end-to-end as predicted and are separated by 24 Å with a symmetry-related duplex region inserted between them (cyan). (B) Stacking interactions between T_{19} of the central duplex and A_6 of the flanking duplexes stabilize the relative position of the helices. CoHex2 positioned in the major groove of the violet duplex also contacts C_{18} phosphate to provide electrostatic stabilization between the tightly packed duplex regions.

Lattice Connectivity from Helical Sheets. One major difference between this designed crystal structure and the template on which it was modeled was the transition to a lower symmetry space group. The nonamer structure crystallized in a tetragonal space group ($I4_122$), with the axis of the coaxially stacked duplexes coincident with the four-fold crystallographic axis, resulting in helical columns that assemble into a 3D DNA lattice through the stacking of the noncanonical regions. The differences in crystal packing of the duplex regions for the crystals described here coincide with crystallization in a lower symmetry orthorhombic space group ($I222$). As a result, instead of forming helical columns, the duplex region forms helical sheets. These are composed of two sets of duplexes that run along the *a*, *b* face diagonals and are woven together to form helical sheets ~26 Å in thickness (Figure 7A). Repeating layers are held together by the noncanonical junction regions that extend out of the top and bottom of each sheet to generate a 3D lattice (Figure 7B). Because the noncanonical interactions all reside along the *c* axis, the distance between the sheets varied by ~6 Å per sheet (12 Å per cell) depending on the pH at which the crystals were grown.

The crystal structures described here are the first that are composed of A-form helical segments and organized out of 2D sheets. This results in a considerably greater density of DNA than in the columnar helical crystals, and this is likely responsible, at least in part, for the relatively high resolution of these structures. Unfortunately, this higher DNA density precludes their use as macromolecular scaffolds, but these crystals may be useful as scaffolds for small molecules. Further, these 2D sheets superficially resemble planar DNA origami sheets,[27] particularly in their thickness, and raises the intriguing possibility that this or similar noncanonical motifs may be useful for supramolecular organization of DNA origami sheets into periodic layered 3D objects.

Noncanonical Junctions in Crystal Design and As Adaptive Materials. The usefulness of noncanonical DNA motifs for creating crystals hinges on predictability. To date, only a handful of predictable noncanonical DNA motifs have been characterized, and one future challenge will be to identify more motifs that form predictable local product structures in the context of longer sequences. By identifying new motifs, structural libraries can be developed to allow for modular assembly of a variety of periodic or nonperiodic structures,

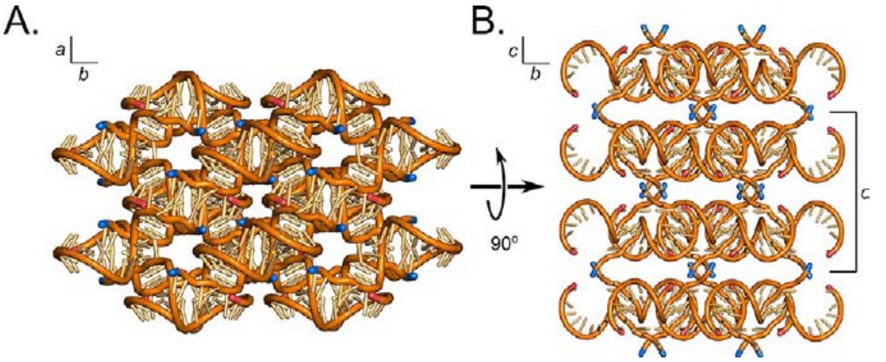

Figure 7. 3D Lattice assembly from 2D helical sheets. Cartoon representation of the pH 7.0 lattice structure with the 5′-end of each strand capped in blue and the 3′-end capped in red. (A) The interwoven duplexes form sheets of helices with the helical axes running parallel to the *a, b* face diagonals. (B) Layers of helical sheets are held together through the parallel-stranded noncanonical region formed by the first 5 nucleotides of each strand. These noncanonical junction regions extend out of the top and bottom of the sheets. Each unit cell contains two sheets with the distance between the sheets dictated by the pH at which the crystals are grown. Crystals grown at pH 5.5 or below would be expanded by ∼1.3 nm per unit cell due to the formation of the hemiprotonated C•C base pair in the noncanonical junction region.

much like what has been done with RNA junctions.[56−58] The high degree of similarity between the noncanonical region at pH 5.5 and the nonamer design template shows that the 5′-CGAA motif can form a predictable structural element in different sequence contexts. However, one of the nonideal features of the original homoparallel 5′-CGAA junction design is the reliance on stacking interactions between C•C base pairs. Hydrogen bonding continuity between each strand that makes up such a motif would be highly desirable for promoting self-assembly and rigidity. Because the C•C junctions are positioned only by stacking, it is likely that lattice strain, either induced by cryocooling or inherent to the lattice, could be accommodated by rotation or sliding of the stacked pairs, resulting in less order and poorer overall electron density. The better density observed for the pH 7.0 noncanonical region with C−G•G−C stacked junctions likely arises from a more defined orientation established by the interstrand base pairing interactions of the quadruple base pairs. This newly discovered motif variant may provide a new tool in the DNA construction kit.

The pH-dependent structural changes observed in these crystals provide new clues about the dynamics of the 5′-CGAA motif. Previous analysis of isolated 5′-d(CGAA) oligonucleotide crystals suggested that this homoparallel motif formed independently of pH and that the hemiprotonated C•C base pair was observed even at pH 7.0.[49] However, solution studies of 5′-CGA containing oligonucleotides showed spectroscopically that the formation of parallel-stranded structures was highly pH-dependent.[47,48] The dramatic differences in pH dependence between the crystal and solution studies might arise from sequence-specific effects, such as the additional A•A pair in the crystals that could provide stabilization, or from the stacking interactions that may be favored during crystallization. The two distinct noncanonical junctions observed in our crystals at acidic and neutral pH's suggest that the other parallel noncanonical base pairs can form in the absence of the hemiprotonated C•C base pair, but that formation of the C•C base pair is pH dependent. Importantly, the multicrystal diffraction observed at intermediate pH's and during pH-induced transitions indicates that the two junctional motifs can coexist in a single crystal. This opens the possibility that the hemiprotonated C•C base pair structure observed at pH 7.0 could have been selectively crystallized out of a population of structural motifs and that this distribution may have contributed to the reported twinning of these crystals.[49]

Our results show that the 5′-CGAA motif is structurally modular in response to pH, and this feature may open unique avenues for creating adaptive biomaterials. The motif is responsive to the pH during crystal growth, and the ability to precisely control unit cell dimensions during this process is a potentially powerful tool for DNA crystal design. Further, our results show that the 5′-CGAA motif is capable of interconversion between the two structures within individual crystals. The interconversion occurs fairly rapidly under our experimental conditions, but for the transition from C−G•G−C stacked junctions to C•C stacked junctions we could directly observe the motif transition through concerted changes in X-ray diffraction over time. To our knowledge, this is the first example of adaptive structural changes observed in DNA crystals and may provide new functionalities for DNA crystals as adaptive biomaterials. For nanotechnology applications, this feature may be useful as a method for locking "guest" molecules into a crystal lattice after they have been absorbed by shrinking the crystal's solvent channels. This may also be a useful feature in crystals or other ordered assemblies for changing or tuning the optical property through modifying the separation distance between repeating units in response to pH.

■ CONCLUSIONS

Despite having well-understood self-assembly properties, constructing periodic 3D DNA crystals that diffract to high resolution remains a difficult task. Noncanonical base pairing motifs offer great promise for adding tools to the DNA nanotechnology construction kit. The crystal structures described here take an important step in establishing the predictability of the 5′-CGAA homoparallel motif, while also revealing a new variation on this motif. The ability to dynamically control this motif by pH fluctuations may open up possibilities of using it to create adaptive 3D biomaterials. Another striking observation from these structures is the large impact that sequence choices for Watson−Crick regions in the design phase can have on DNA crystal assembly. Though DNA base pairs are generally considered isostructural when used for construction on the nanoscale, our results demonstrate that this may be a poor assumption from a crystal design perspective where interactions with the crystallization environment can have a large impact on its ability to crystallize or on the resulting lattice structures. Though the crystals did not entirely meet our design expectations, these are the first designed DNA lattices determined at better than 2.0 Å. These high resolution structures provide important insights into DNA crystal design and construction and can serve as a new template for improved 3D DNA crystal design.

EXPERIMENTAL SECTION

Synthesis and Purification. The oligonucleotide, d-(GCGAAAGGGCACGTGCCCT), was synthesized using standard solid state chemistry (IDT Technologies, Coralville, IA) and purified by denaturing 20% (w/v) 19:1 acrylamide/bis-acrylamide, 7 M urea gel electrophoresis, electro-elution, and ethanol precipitation. The dried oligonucleotide was dissolved in 5 mM sodium cacodylate (pH 7.0), and the concentration was determined by absorbance at 260 nm using an extinction coefficient of 179 100 L/mol·cm.

Crystallization. Crystals were grown by vapor diffusion in sitting drops. 3 μL of DNA (300 μM) were mixed with 1 μL of the well solution containing 14 mM magnesium chloride, 65 mM sodium chloride, 21 mM cobalt(III) hexammine, 28 mM sodium cacodylate (pH 5.5−7.4) or sodium acetate (pH 4.5−5.5) of varying pHs, and 17.5% (v/v) 2-methyl-2,4-pentanediol and incubated at 37 °C overnight followed by cooling to 24 °C. Clusters of thin crystal plates grew in 1−2 days following the transfer to 24 °C. Individual crystals within clusters varied in size from ∼50 to ∼300 μm in the longest dimension and remained stable within the drops over the course of several weeks.

Data Collection. Single crystals were removed from the equilibrated drops and flash cooled directly in the nitrogen cold stream at 100 K or mounted with MiTeGen (Ithaca, NY) MicroRT loops and capillaries with 45 μL of crystallization well solution in the reservoir. Data were collected on a Brüker Proteum Platinum[135] CCD detector with a Brüker Microstar-HF X-ray source equipped with Helios optics. Data sets for structure determination were collected in two passes on a single crystal to generate high and low resolution data sets that were then indexed, integrated, and scaled in HKL-2000.[59] Crystals observed at room temperature were aligned with the c^* axis in the diffraction plane. Vapor-induced pH changes were initiated by exchanging the MiTeGen capillary with a new capillary containing 45 μL of reservoir solution supplemented with 0.1 M acetic acid or ammonium hydroxide. Care was taken to prevent the crystal from shifting position during the exchange.

Structure Determination and Refinement. Initial phase estimates were generated from the positions of cobalt atoms found by single wavelength anomalous dispersion and density modification using Phenix.[60] Experimental electron density maps were of sufficient quality to clearly make out the A-form helices and nucleobase density of residues in the noncanonical region. The structure was built using Coot[61] and refined with Refmac5.[62] Test set reflections (4.5%) were randomly chosen for the pH 7.0 data, and the same test set was used for the structure determined at pH 5.5. Final R and R_{free} values are given in Table S1. The relatively large difference between R and R_{free} values (0.07) for the pH 7.0 structure was consistent throughout the refinement process.

ASSOCIATED CONTENT

Supporting Information

Table S1 and Figures S1−S3. This material is available free of charge via the Internet at http://pubs.acs.org.

AUTHOR INFORMATION

Corresponding Author

paukstel@umd.edu

Notes

The authors declare no competing financial interest.

ACKNOWLEDGMENTS

This work was supported by an NSF CAREER award to P.J.P. (1149665). Coordinates and structure factors have been deposited in the Protein Data Bank with IDs 4F8G and 4F8I.

REFERENCES

(1) Winfree, E.; Liu, F.; Wenzler, L. A.; Seeman, N. C. *Nature* **1998**, *394*, 539−44.
(2) Shih, W. M.; Quispe, J. D.; Joyce, G. F. *Nature* **2004**, *427*, 618−21.
(3) Ding, B.; Sha, R.; Seeman, N. C. *J. Am. Chem. Soc.* **2004**, *126*, 10230−1.
(4) Mitchell, J. C.; Harris, J. R.; Malo, J.; Bath, J.; Turberfield, A. J. *J. Am. Chem. Soc.* **2004**, *126*, 16342−3.
(5) He, Y.; Chen, Y.; Liu, H.; Ribbe, A. E.; Mao, C. *J. Am. Chem. Soc.* **2005**, *127*, 12202−3.
(6) Liu, Y.; Ke, Y.; Yan, H. *J. Am. Chem. Soc.* **2005**, *127*, 17140−1.
(7) Liu, H.; Chen, Y.; He, Y.; Ribbe, A. E.; Mao, C. *Angew. Chem., Int. Ed.* **2006**, *45*, 1942−5.
(8) Lin, C.; Liu, Y.; Rinker, S.; Yan, H. *ChemPhysChem* **2006**, *7*, 1641−7.
(9) Zheng, J.; Birktoft, J. J.; Chen, Y.; Wang, T.; Sha, R.; Constantinou, P. E.; Ginell, S. L.; Mao, C.; Seeman, N. C. *Nature* **2009**, *461*, 74−77.
(10) Rothemund, P. W. K.; Papadakis, N.; Winfree, E. *PLoS Biol* **2004**, *2*, e424.
(11) Mao, C.; LaBean, T. H.; Relf, J. H.; Seeman, N. C. *Nature* **2000**, *407*, 493−6.
(12) Yan, H.; Feng, L.; LaBean, T. H.; Reif, J. H. *J. Am. Chem. Soc.* **2003**, *125*, 14246−7.
(13) Barish, R. D.; Rothemund, P. W. K.; Winfree, E. *Nano Lett* **2005**, *5*, 2586−92.
(14) Yan, H.; Park, S. H.; Finkelstein, G.; Reif, J. H.; LaBean, T. H. *Science* **2003**, *301*, 1882−4.
(15) Mitra, D.; Di Cesare, N.; Sleiman, H. F. *Angew. Chem., Int. Ed.* **2004**, *43*, 5804−8.
(16) Sharma, J.; Chhabra, R.; Liu, Y.; Ke, Y.; Yan, H. *Angew. Chem., Int. Ed.* **2006**, *45*, 730−5.
(17) Chhabra, R.; Sharma, J.; Liu, Y.; Yan, H. *Adv. Exp. Med. Biol.* **2007**, *620*, 107−16.
(18) Stearns, L. A.; Chhabra, R.; Sharma, J.; Liu, Y.; Petuskey, W. T.; Yan, H.; Chaput, J. C. *Angew. Chem., Int. Ed.* **2009**, *48*, 8494−8496.
(19) Seeman, N. C. *J. Theor. Biol.* **1982**, *99*, 237−47.
(20) Ariga, K.; Hill, J. P.; Ji, Q. *Macromol. Biosci.* **2008**, *8*, 981−990.
(21) You, J.-O.; Almeda, D.; Ye, G. J.; Auguste, D. T. *J. Biol. Eng.* **2010**, *4*, 15.
(22) Stuart, M. A. C.; Huck, W. T. S.; Genzer, J.; Müller, M.; Ober, C.; Stamm, M.; Sukhorukov, G. B.; Szleifer, I.; Tsukruk, V. V.; Urban, M.; Winnik, F.; Zauscher, S.; Luzinov, I.; Minko, S. *Nat. Mater.* **2010**, *9*, 101−113.
(23) Costa, D.; Miguel, M. G.; Lindman, B. *Adv. Colloid Interface Sci.* **2010**, *158*, 21−31.
(24) Sun, T.; Qing, G. *Adv. Mater. Weinheim* **2011**, *23*, H57−77.
(25) Seeman, N. C. *Nature* **2003**, *421*, 427−31.
(26) Seeman, N. C. *Annu. Rev. Biophys. Biomol. Struct.* **1998**, *27*, 225−48.
(27) Rothemund, P. W. K. *Nature* **2006**, *440*, 297−302.
(28) Andersen, E. S.; Dong, M.; Nielsen, M. M.; Jahn, K.; Subramani, R.; Mamdouh, W.; Golas, M. M.; Sander, B.; Stark, H.; Oliveira, C. L. P.; Pedersen, J. S.; Birkedal, V.; Besenbacher, F.; Gothelf, K. V.; Kjems, J. *Nature* **2009**, *459*, 73−76.
(29) Douglas, S. M.; Dietz, H.; Liedl, T.; Hogberg, B.; Graf, F.; Shih, W. M. *Nature* **2009**, *459*, 414−418.
(30) Dietz, H.; Douglas, S. M.; Shih, W. M. *Science* **2009**, *325*, 725−730.
(31) Endo, M.; Hidaka, K.; Kato, T.; Namba, K.; Sugiyama, H. *J. Am. Chem. Soc.* **2009**, *131*, 15570−15571.

(32) Ke, Y.; Douglas, S. M.; Liu, M.; Sharma, J.; Cheng, A.; Leung, A.; Liu, Y.; Shih, W. M.; Yan, H. *J. Am. Chem. Soc.* **2009**, *131*, 15903−15908.

(33) Liedl, T.; Hogberg, B.; Tytell, J.; Ingber, D. E.; Shih, W. M. *Nat. Nano.* **2010**, *5*, 520−524.

(34) Han, D.; Pal, S.; Nangreave, J.; Deng, Z.; Liu, Y.; Yan, H. *Science* **2011**, *332*, 342−346.

(35) Seeman, N. C. *Nat. Comput.* **2002**, *1*, 53−84.

(36) Westhof, E.; Fritsch, V. *Structure* **2000**, *8*, R55−65.

(37) Sundquist, W. I.; Klug, A. *Nature* **1989**, *342*, 825−9.

(38) Siddiqui-Jain, A.; Grand, C. L.; Bearss, D. J.; Hurley, L. H. *Proc. Natl. Acad. Sci. U.S.A.* **2002**, *99*, 11593−8.

(39) Alberti, P.; Mergny, J.-L. *Proc. Natl. Acad. Sci. U.S.A.* **2003**, *100*, 1569−73.

(40) Chen, Y.; Lee, S.-H.; Mao, C. *Angew. Chem., Int. Ed.* **2004**, *116*, 5449−5452.

(41) Surana, S.; Bhat, J. M.; Koushika, S. P.; Krishnan, Y. *Nat. Commun.* **2011**, *2*, 340.

(42) Saha, S.; Chakraborty, K.; Krishnan, Y. *Chem. Commun. (Camb.)* **2012**, *48*, 2513−2515.

(43) Paukstelis, P. J.; Nowakowski, J.; Birktoft, J. J.; Seeman, N. C. *Chem. Biol.* **2004**, *11*, 1119−26.

(44) Paukstelis, P. J. *J. Am. Chem. Soc.* **2006**, *128*, 6794−5.

(45) Kettani, A.; Bouaziz, S.; Skripkin, E.; Majumdar, A.; Wang, W.; Jones, R. A.; Patel, D. J. *Structure* **1999**, *7*, 803−15.

(46) Sunami, T.; Kondo, J.; Kobuna, T.; Hirao, I.; Watanabe, K.; Miura, K.; Takénaka, A. *Nucleic Acids Res.* **2002**, *30*, 5253−60.

(47) Robinson, H.; van der Marel, G. A.; van Boom, J. H.; Wang, A. H. *Biochemistry* **1992**, *31*, 10510−7.

(48) Robinson, H.; Wang, A. H. *Proc. Natl. Acad. Sci. U.S.A.* **1993**, *90*, 5224−8.

(49) Kobuna, T.; Sunami, T.; Kondo, J.; Takénaka, A. *Nucleic Acids Res. Suppl.* **2002**, 179−80.

(50) Lu, X.-J.; Olson, W. K. *Nat. Protoc.* **2008**, *3*, 1213−1227.

(51) Franklin, R. E.; Gosling, R. G. *Nature* **1953**, *171*, 740−741.

(52) Braunlin, W. H.; Xu, Q. *Biopolymers* **1992**, *32*, 1703−1711.

(53) Xu, Q.; Shoemaker, R. K.; Braunlin, W. H. *Biophys. J.* **1993**, *65*, 1039−1049.

(54) Robinson, H.; Wang, A. H. *Nucleic Acids Res.* **1996**, *24*, 676−682.

(55) Bauer, C.; Wang, A. H. *J. Inorg. Biochem.* **1997**, *68*, 129−135.

(56) Yingling, Y. G.; Shapiro, B. A. *Nano Lett.* **2007**, *7*, 2328−2334.

(57) Bindewald, E.; Grunewald, C.; Boyle, B.; O'Connor, M.; Shapiro, B. A. *J. Mol. Graph. Model.* **2008**, *27*, 299−308.

(58) Bindewald, E.; Hayes, R.; Yingling, Y. G.; Kasprzak, W.; Shapiro, B. A. *Nucleic Acids Res.* **2008**, *36*, D392−397.

(59) Otwinowski, Z.; Minor, W. *Methods Enzymol.* **1997**, *276*, 307−326.

(60) Adams, P. D.; Afonine, P. V.; Bunkóczi, G.; Chen, V. B.; Echols, N.; Headd, J. J.; Hung, L.-W.; Jain, S.; Kapral, G. J.; Grosse Kunstleve, R. W.; McCoy, A. J.; Moriarty, N. W.; Oeffner, R. D.; Read, R. J.; Richardson, D. C.; Richardson, J. S.; Terwilliger, T. C.; Zwart, P. H. *Methods* **2011**, *55*, 94−106.

(61) Emsley, P.; Lohkamp, B.; Scott, W. G.; Cowtan, K. *Acta Crystallogr., Sect. D* **2010**, *66*, 486−501.

(62) Murshudov, G. N.; Vagin, A. A.; Dodson, E. J. *Acta Crystallogr., Sect. D* **1997**, *53*, 240−255.